Biochemistry

 Volume 37, Number 35 September 1, 1998

Accelerated Publications

Crystal Structure of an Eight-Base Pair Duplex Containing the 3′-DNA−RNA-5′ Junction Formed during Initiation of Minus-Strand Synthesis of HIV Replication†

Uwe Mueller,‡ Gottfried Maier,§ Alberto Mochi Onori,|| Luciano Cellai,|| Hermann Heumann,§ and Udo Heinemann*,‡,⊥

Forschungsgruppe Kristallographie, Max-Delbrück-Centrum für Molekulare Medizin, Robert-Rössle-Strasse 10, D-13122 Berlin, Germany, Max-Planck-Institut für Biochemie, Am Klopferspitz 18A, D-82152 Martinsried, Germany, Instituto di Strutturistica Chimica, CNR, P.O. Box 10, I-00016 Monterotondo Stazione, Italy, and Institut für Kristallographie, Freie Universität Berlin, Takustrasse 6, D-14195 Berlin, Germany

Received May 18, 1998; Revised Manuscript Received July 1, 1998

ABSTRACT: During initiation of minus-strand synthesis by HIV-1 reverse transcriptase, a 3′-DNA−RNA-5′ junction is formed involving the 3′-end of $tRNA^{lys,3}$. The HIV-RT-associated RNase H cleaves the RNA template strand specifically, opposite the newly synthesized DNA strand. We have determined the crystal structure at 1.9 Å resolution of an eight-base pair hybrid duplex representing the junction to identify global or local structural perturbations which may be recognized by HIV-RT RNase H. The junction octamer is in a global A-type conformation throughout. A base pair step with distinct stacking geometry and variable backbone conformation is located next to the main endonucleolytic cleavage site. This base pair step may serve as a recognition site for HIV-RT RNase H.

Replication of HIV is catalyzed by reverse transcriptase in two steps. First, a DNA strand (the minus strand) complementary to the viral RNA genome is synthesized. This strand serves as a template for synthesis of the second DNA strand (the plus strand). Both processes, minus-strand synthesis as well as plus-strand synthesis, are initiated by RNA primers (*1*). Extension of these primers by HIV reverse transcriptase (HIV-RT)[1] leads to formation of a 5′-RNA−DNA-3′ junction. The question of whether these RNA−DNA junctions act as recognition sites for HIV-RT-associated RNase H has been previously analyzed with respect to the junction formed by $tRNA^{lys,3}$ during initiation of minus-strand synthesis (*2*, *3*).

$tRNA^{lys,3}$ binds with its 3′-end to a complementary region of the viral RNA, the primer binding site (PBS), facilitating initiation of minus-strand synthesis (Figure 1a). Extension of the RNA primer by HIV-RT leads to formation of a 5′-RNA−DNA-3′ junction in the primer strand, while the template strand is uniformly RNA. It has been shown that HIV-RT-associated RNase H cuts the RNA template opposite

† Supported by the Deutsche Forschungsgemeinschaft under Grants He 1318/12 (U.H.) and He 1285/8 (H.H.) and the Fonds der Chemischen Industrie.

* To whom correspondence should be addressed: FG Kristallographie, Max-Delbrück-Centrum für Molekulare Medizin, Robert-Rössle-Strasse 10, D-13122 Berlin, Germany. Telephone: +49 30 9406 3420. Fax: +49 30 9406 2548. E-mail: heinemann@mdc-berlin.de.

‡ Max-Delbrück-Centrum für Molekulare Medizin.

§ Max-Planck-Institut für Biochemie.

|| Instituto di Strutturistica Chimica, CNR.

⊥ Freie Universität Berlin.

[1] Abbreviations: HIV-RT, HIV-1 reverse transcriptase; MPD, 2-methyl-2,4-pentanediol; NCS, noncrystallographic symmetry; PBS, primer binding site; rmsd, root-mean-square deviation.

S0006-2960(98)01152-0 CCC: $15.00
Published on Web 08/14/1998

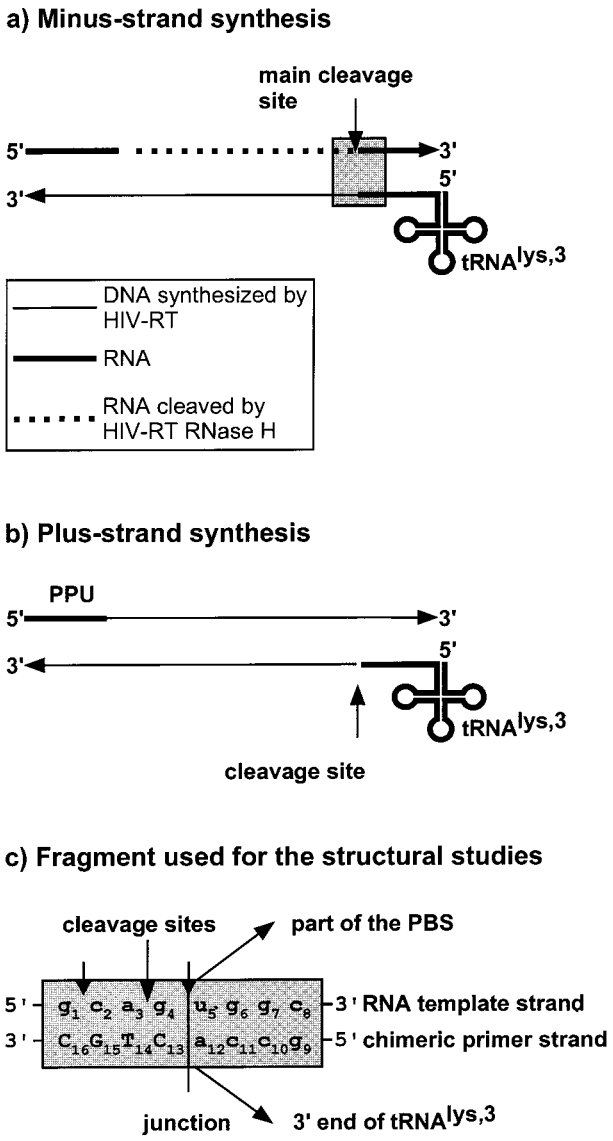

FIGURE 1: Formation and significance of the 3′-DNA−RNA-5′ junction occurring during initiation of minus-strand synthesis. (a) Extension of the $tRNA^{lys,3}$ by HIV-RT leads to formation of the junction. HIV-RT RNase H cleaves the RNA template while DNA synthesis proceeds. (b) During minus-strand synthesis initiated at the polypurine track (PPU), the $tRNA^{lys,3}$ junction-containing strand is the template strand. It is cleaved one base position downstream (in the 5′-direction) of the junction. (c) The sequence of the duplex used for the crystallographic study is shown as shaded area in panels a and c. PBS is the primer binding site. Throughout this paper, uppercase letters represent deoxyribonucleotides and lowercase letters ribonucleotides.

this RNA−DNA junction endonucleolytically and digests the template RNA exonucleolytically in the 5′-direction. The main cleavage site lies between base positions +1 and +2 (counting from the junction in the 5′-direction), and two minor cleavage sites are observed between positions +1 and −1 (exactly at the junction) and between positions +3 and +4 (*3*), as indicated in Figure 1c.

For the synthesis of the second (plus) strand, the minus strand is the template strand (Figure 1b). Thus, the $tRNA^{lys,3}$ junction is located in the template strand. It has been previously shown (*2*) that in this case the minus-strand DNA is separated from the $tRNA^{lys,3}$ primer by an RNase H cut one base position in the 5′-direction from the junction. The structure of this junction which represents the primer−template combination during plus-strand synthesis has previously been studied by NMR spectroscopy (*4*). It has been claimed that the width of the minor groove is the structural determinant for cleavage.

Table 1: Diffraction Data and Refinement Statistics

space group	$P2_12_12_1$
cell parameters (Å)	$a = 42.74$, $b = 44.15$, $c = 51.93$
radiation source	DESY BW7A/X31
wavelength (Å)	1.000/1.072
resolution range (Å)	15−1.94
temperature during experiment (K)	100
crystal mosaicity (deg)	0.9/0.8
no. of unique observations	7566
completeness[a] (%)	99.2/93.1
multiplicity	3.7
$\langle I/\sigma(I)\rangle^{a,b}$	7.4/2.2
$R_{sym}^{a,c}$ (%)	7.5/41.6
no. of molecules per asymmetric unit	two duplexes
final R/R_{free}^{d} (%)	21.6/29.8
no. of RNA atoms	666
no. of water oxygen atoms	86
rmsd[e] bond lengths to library (Å)	0.012
rmsd[e] bond angles to library (deg)	1.69

[a] Resolution shells of 15−1.94 and 1.96−1.94 Å. [b] I is the reflection intensity. [c] $R_{sym} = 100(\Sigma_{h,i}|I_{h,i} - I_h|/\Sigma_{h,i}I_{h,i})$ where the summation is over all observations $I_{h,i}$ contributing to the reflection intensities I_h. [d] R_{free} based on 5% of the data selected from thin resolution shells with DATAMAN (*11*). [e] rmsd is the root-mean-square deviation.

In this study, we have analyzed the structure of the $tRNA^{lys,3}$ junction formed during initiation of minus-strand synthesis (Figure 1c). We have determined the crystal structure of an eight-base pair duplex consisting of four base pairs of dsRNA and four base pairs of the DNA−RNA hybrid. The pure RNA strand (lowercase letters) contains part of the PBS, and the complementary strand is a chimeric fragment with the 5′-terminus consisting of four ribonucleotides from the 3′-end of the $tRNA^{lys,3}$ and with the 3′-terminus consisting of four deoxyribonucleotides (uppercase letters) from the minus strand.

MATERIALS AND METHODS

Sample Preparation. The synthesis and purification of the duplex used for crystallization have been described elsewhere (T. Szyperski, G. Maier, A. Mochi Onori, L. Cellai, H. Heumann, and K. Wüthrich, submitted for publication). After hybridization with a 0.5 mM strand concentration, residual single strands were separated from the hybrid duplex by anion exchange chromatography on a Pharmacia (Uppsala, Sweden) FPLC system using a MonoQ column. The duplex was eluted in a buffer of 20 mM Tris/HCl (pH 8.0) and 5 mM magnesium chloride by applying a linear gradient from 0 to 1 M sodium chloride and desalted on a Bio Gel P6 column. Crystallization at 20 °C applying the hanging drop vapor diffusion method and using a buffer screen optimized for short nucleic acid duplexes (*5*) gave crystals under several conditions after 2−4 weeks. The best crystals grew when 1.5 μL of the 0.5 mM hybrid duplex was mixed with 1.5 μL of 40 mM sodium cacodylate (pH 7.0), 12 mM spermine tetrahydrochloride, 20 mM potassium chloride, and 10% (by volume) 2-methyl-2,4-pentanediol (MPD) and equilibrated against a reservoir consisting of 500 μL of 35% (by volume) MPD. Due to the high MPD concentration in the droplet

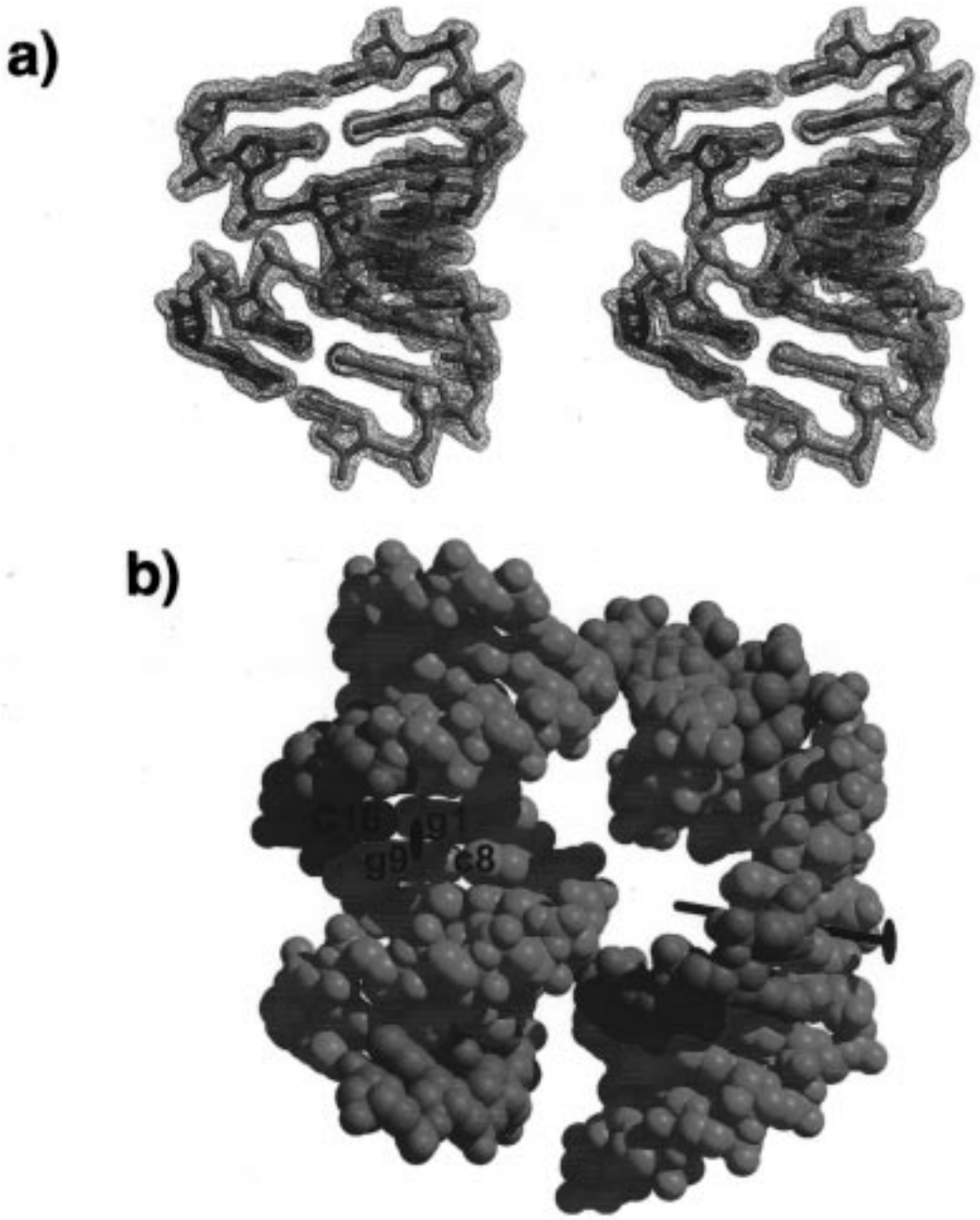

FIGURE 2: Crystal structure of the DNA−RNA junction octamer with RNA nucleotides shown in green and DNA in red. (a) Stereodrawing of the DNA−RNA juction duplex with $2F_o - F_c$ difference density contoured at 0.9σ. Only density within 1.8 Å of the displayed atoms is shown. The minor groove is on the right-hand side, and the major groove is to the left. (b) Crystal packing motifs for the junction octamer. Two pairs of octamers, stacked end to end to form 16-base pair helices, interact with contacts between terminal base pairs and the minor groove. The 16-base pair helix is the asymmetric unit of the crystal. Its central base pair step displays left-handed twist with perfect stacking between the RNA guanines g1 and g9 and almost complete unstacking of cytosines c8 and C16. The central pseudo-2-fold axis of the 16-base pair helix relates the four DNA nucleotides to RNA nucleotides and vice versa, since the duplexes stack head to tail and not head to head. This figure was prepared with BobScript (*32*) and Raster3D (*33*).

after equilibration, the solution permitted direct mounting of crystals for cryocooling diffraction experiments.

X-ray Data. Diffraction data were measured from two crystals of 500 μm × 100 μm × 50 μm each at a temperature of 100 K at the EMBL Outstation at DESY, Hamburg, using a MAR Research (Hamburg, Germany) imaging plate detector. For the first data set, a total oscillation range of 94° was covered with a ϕ increment of 1° per image and dose-dependent exposures of approximately 5 min on beamline BW7A. The data set was completed at beamline X31 using a second crystal and an exposure of approximately 10 min per frame. Here, the total ϕ range was 44° with 2° increments. Data processing and unit cell and space group determination were carried out with DENZO/SCALEPACK (*6*) (Table 1). Space group $P2_12_12_1$ was confirmed by inspection of systematic absences of every odd reflection along *a**, *b**, and *c**. All crystals displayed high mosaicity of up to 0.9° which was also observed in test exposures without cryocooling. This resulted in an unfavorable ratio of fully observed versus partial reflections during data evaluation. A merged and complete data set was used for structure solution and refinement of the hybrid duplex.

Table 2: Conformational Parameters[a]

		x displacement dx (Å)	inclination η (deg)	tip θ (deg)	twist ω (deg)	rise Dz (Å)	slide Dy (Å)
I	mean	−4.25	10.67	−0.15	33.52	2.77	−0.08
	σ	0.27	2.74	1.47	1.92	0.37	0.34
II	mean	−4.66	15.63	−4.10	32.80	2.65	−0.15
	σ	0.22	4.38	1.11	2.81	0.28	0.33
RNA	mean	−4.61	11.26	−2.18	32.83	2.68	−0.21
	σ	0.22	2.68	1.49	1.33	0.25	0.33
RNA−DNA	mean	−4.28	15.04	−2.08	33.29	2.73	−0.12
	σ	0.33	5.03	3.17	3.47	0.34	0.34
junction	mean				33.75	2.62	0.20
	σ				0.80	0.16	0.04
fiber[b]	mean	−5.14	22.66	0.00	32.70	2.55	0.00
correlation of I/II		0.53	0.06	−0.61	0.76	0.48	0.78

[a] Calculated with CURVES (*34*). Mean values and their standard deviations are shown for selected parameters in the two independent molecules I and II, the RNA parts in both molecules, the RNA−DNA hybrid parts in both molecules, and the base pair steps at the junction. [b] Coordinates for calf thymus DNA in the A conformation (*35*).

Structure Solution and Refinement. Packing considerations suggested the presence of two octamer duplexes per asymmetric unit of the orthorhombic cell yielding a volume per nucleotide pair (*7*) of 1531 Å^3. The structure of the hybrid octamer duplex was solved by molecular replacement with AMORE (*8*) using a canonical A-RNA model with the appropriate sequence. The cross-rotation function was solved using data between 8 and 3 Å. Four different solutions appearing at 3.9−3.3σ were selected for translation searches using data from 8 to 4 Å. The best solution in this translation function yielded an *R* value of 54.6% and a correlation coefficient of 0.222 which improved to 53.4% and 0.273, respectively, after rigid body refinement against 8−4 Å data. This solution was kept fixed in further translation searches using the remaining solutions of the rotation function. After additional rigid body refinement and model inspection using O (*9*), the two correctly packed model octamers gave an *R* value of 48.9% and a correlation coefficient of 0.410.

Prior to the start of the refinement, the search model was edited to remove all O2′ atoms from the deoxy stretches of both duplexes. For the calculation of R_{free} (*10*), 5% of the data were randomly chosen by the program DATAMAN (*11*) within thin resolution shells to avoid bias of the cross-validation procedure due to noncrystallographic symmetry (NCS). Initial rigid body refinement and step by step positional refinement with data up to 2.5 Å applying tight NCS restraints for both helices improved the model with an R/R_{free} of 36.8%/43.4%. $2F_o - F_c$ and $F_o - F_c$ maps now showed positive and negative difference electron density at several ribose O2′ positions, indicating that one duplex had to be rotated by 180° around the pseudo 2-fold axis perpendicular to the helical axis. After manual model correction, application of the XPLOR (*12*) bulk solvent correction, and further positional and individual *B*-factor refinement, R/R_{free} was reduced to 30.7%/34.9% for all data to 1.94 Å. From here on, cyclic extension of the solvent model together with visual map inspection and further refinement was carried out to convergence at an R/R_{free} value of 21.6%/29.6%. The final $F_o - F_c$ map contoured at 3σ was clear in the nucleic acid region and without interpretable features in the solvent area. The relatively high *R* values are thought to result from the high crystal mosaicity and the weak data at high resolution. Coordinates and structure factor amplitudes are deposited with the Nucleic Acid Data Bank (NDB) under accession code AHH0114.

RESULTS

The 3′-DNA−RNA-5′ Junction Adopts a Global A Conformation. The junction octamer r(gcaguggc)·r(gcca)d(CTGC) is present in two independent copies (I and II) in the asymmetric unit of the crystal. Both molecules are unambiguously defined by electron density. They adopt an A-type conformation throughout their entire length (Figure 2a). In the crystal, two hybrid duplexes pack head to tail to form 16-base pair double helices with negative twist (ω = −19.4°) at the central stack lacking the connecting phosphodiester bonds (Figure 2b). This particular stacking geometry gives the 16-base pair unit a wide open major groove uncharacteristic of the A form. Other crystal contacts arise from the fitting of terminal base pairs into the flat minor grooves of neighboring molecules, as is frequently observed in crystal structures of DNA or RNA duplexes in the A form (*7*, *13*−*16*).

In the junction octamer, the A form is clearly apparent from the C3′-endo sugar pucker uniformly present in all 32 nucleotides of the asymmetric unit and from the average helical parameters (Table 2). In particular, the x displacement of base pairs leading to a deep major groove, the considerable inclination of base pairs against the helix axis, the concomitantly small rise per base pair, and the mean twist values of the two molecules of 33.5 and 32.8°, corresponding to helix repeats of 10.7 and 11.0 base pairs per turn, are indicative of a standard A conformation. After least-squares superposition of all equivalent atoms, the two independent duplexes deviate with an rmsd of 1.01 Å from each other and with rmsds of 0.95 and 0.84 Å, respectively, from the standard A-form fiber model with the identical sequence. Molecule I differs from II mainly by a smaller average magnitude of displacement (dx = −4.25 vs −4.66 Å), a smaller mean inclination (η = 10.7 vs 15.6°), and a smaller average magnitude of tip (θ = −0.2 vs −4.1°). The differences in conformation between the two copies of the junction octamer are mainly attributed to the effects of crystal packing and, to a lesser extent, to model error.

The two hybrid octamers display a global A conformation throughout. There are no systematic differences in helix geometry between the four base pairs per molecule of pure RNA duplex and the four base pairs of RNA−DNA hybrid duplex. Deviations between mean helix parameters in the RNA and hybrid parts are smaller than or of the same

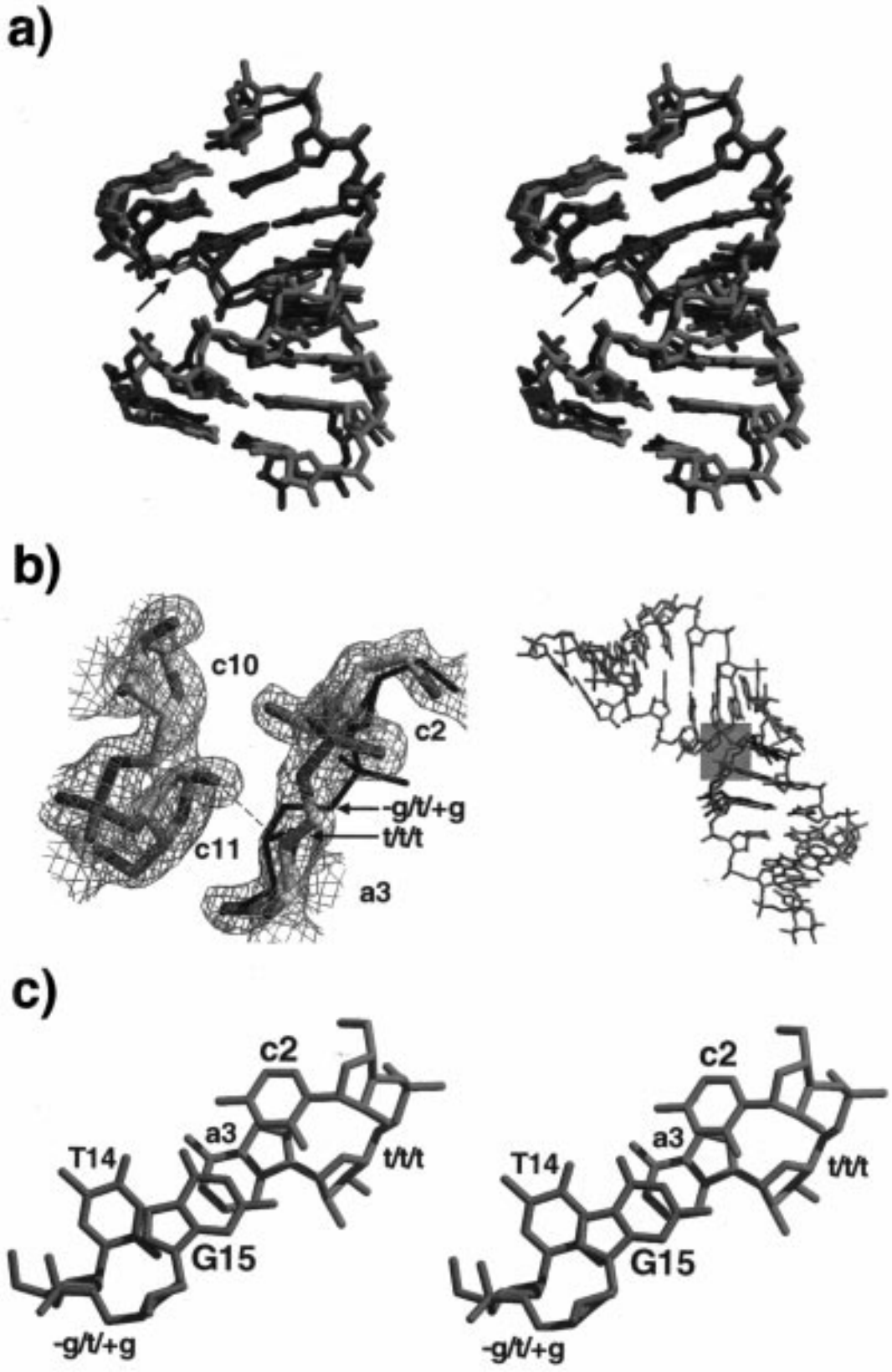

FIGURE 3: Base pair stacking and unusual backbone conformation at the c*p*a·T*p*G step of the junction octamer. RNA nucleotides are shown in green and DNA in red. (a) Least-squares superposition of the two independent molecules in the crystal. Only the four base pairs of the RNA−DNA hybrid part of the duplex (top half) were used in the fit. The arrow points at the extended backbone between nucleosides c2 and a3 of molecule II (lighter hues). (b) Extended backbone between c2 and a3 of molecule II ($\alpha\beta\gamma$ all-trans) with $2F_o - F_c$ electron density contoured at 1.5σ (left). A crystal contact (broken line) would lead to a severe clash if the backbone were in the standard (−)-gauche, trans, (+)gauche conformation as in molecule I (black lines, from the superposition shown in panel a). (Right) Two octamer helices in the crystal lattice. The contact shown in detail at the left is highlighted in pink. (c) Base pair stacking between c2-G15 and a3-T14 shows cross-strand overlap between purine bases and intrastrand unstacking in both the RNA and DNA chain. This figure was prepared with BobScript (*32*) and Raster3D (*33*).

magnitude as differences between independent molecules I and II (see Table 2). According to this crystal structure, there is, thus, no significant difference in global conformation between the pure RNA duplex and the RNA−DNA hybrid duplex which could be sensed by the HIV-RT RNase H. In particular, with 10.1 ± 0.4 Å, the minor groove width is the same in both halves of the double helix.

Junction Recognition and Strand Cleavage by the HIV-RT RNAse H. The two independent copies present in the crystal provide a convenient means of assessing the significance of variations in structural parameters along the hybrid duplexes. The degree of variation is apparent from the standard deviations from the mean values given in Table 2. If these structural variations were predominantly determined by the nucleotide sequence, they should be the same in both molecules I and II. The changes in parameter values should be correlated. Inspection of linear correlation coefficients shows that only twist and slide are moderately correlated, whereas the other helical parameters change more or less independently over the length of the two double helices. The base pair step clearly showing up as unusual in an analysis of helical parameters is the second from the end, c*p*a·T*p*G, which features local minima of twist (30.8 and 28.2°), slide (−0.34 and −0.65 Å), and rise (2.43 and 2.08 Å) in both molecules. In molecule II, this stacking pattern is accompanied by an unusual, extended $\alpha\beta\gamma$ all-trans backbone conformation of nucleotide a3 (Figure 3). This type of stacking, leading to cross-strand overlap of purine bases, along with the extended sugar phosphate backbone has been observed frequently at pyrimidine-purine steps in A-form double helices (*13*, *16*, *17*). The fact that the backbone is extended only on one side and only in one of the two c*p*a·T*p*G steps appears to indicate that the cross-strand base pair stacking lowers the energy barrier between two alternative backbone conformations without necessarily driving the structure all the way to the all-trans form. In this view, the c*p*a·T*p*G step is a conformational soft spot. In fact, the extended backbone is correlated with crystal packing, since a backbone in the usual $\alpha\beta\gamma$ [(−)gauche, trans, (+)gauche] conformation of molecule II would clash with a neighboring duplex as seen in Figure 3b.

DISCUSSION

Significance of the cpa·TpG Base Pair Step. We have demonstrated that the hybrid duplex r(gcaguggc)·r(gcca)-d(CTGC), representing the HIV-RT RNase H cleavage site formed during minus-strand synthesis, is a standard A-type double helix in the crystal. It may be of functional significance that a structural perturbation at the c*p*a·T*p*G step in the hybrid is flanked by the main cleavage site of HIV-RT RNase H which is located one step downstream and by one of the minor cleavage sites located one step upstream (*3*). Conformational flexibility near the cleavage site, as demonstrated for the c*p*a·T*p*G step, may thus be important for cleavage specificity along with the presence or absence of 2′-hydroxyl groups on the complementary strand. In this respect, it is interesting to note that the second minor cleavage site is again located directly upstream of a pyrimidine-purine step, u*p*g·c*p*a. Base pair steps of this kind are known to be conformationally variable, since intrastrand base stacking is weakened and can be abandoned in exchange for cross-strand stacking (*13*, *16*, *17*) as seen in the c*p*a·T*p*G step.

Structural Features of DNA−RNA Junctions and Hybrids. To the best of our knowledge, this is the first crystal structure of a 3′-DNA−RNA-5′ junction base paired to an RNA strand. A number of crystal structures of DNA−RNA hybrids in other arrangements have been published (*18*−*23*). Consistent with our findings, these analyses tend to demonstrate the absence of global structural differences between the RNA and DNA parts of the molecules. According to the crystal structures, a Watson−Crick base-paired duplex in which one strand consists of RNA or contains a stretch of RNA will be in the A form throughout, unless the sequence directs it into the left-handed Z form (*24*). In some cases, the A form extends into double-helical regions with two DNA strands (*18*−*20*). The single apparent exception to this "all-A-form" principle is the hybrid decamer r(uucgggccgg)·d(GGCGCCCGAA) representing a portion of the primer binding site of HIV-1 reverse transcriptase after completion of plus-strand synthesis and a cleavage site for the HIV-1 RT-associated RNase H (*25*−*27*). In the crystal structure of this duplex (*22*), two consecutive adenosines at the 3′-end of the DNA strand have B-like sugar pucker and confer B-like properties to this end of the helix, whereas the major part of the duplex is in the A form. One reason for this aberration from the pure A conformation may rest in the known tendency of 3′-terminal residues in A-form DNA helices to switch sugar pucker into the S domain of the pseudorotation cycle (*13*). In addition, the specific packing mode of this decamer duplex creating stacked helices with A*p*A-u*p*u·A*p*A-u*p*u junctions may destabilize the A form, since adenine-rich DNA stretches are known to prefer the B conformation (*28*).

In contrast to the crystal structures, NMR studies of model substrates of HIV-1 RNase H (*4*, *29*) and other RNA−DNA hybrids (*30*, *31*) have consistently shown backbone conformations of the deoxyribonucleotides outside the C3′-endo domain. It has been suggested that global structures intermediate between the A and B forms (*30*, *31*) or local perturbations near the RNA−DNA junction (*4*) may be responsible for the cleavage specificities of RNase H molecules. In particular, the width of the minor groove has been implicated in recognition by RNase H (*31*). The crystal structure presented here, showing a purely A-form hybrid duplex with uniform minor groove width, is clearly not consistent with these findings. Whether the presence of a continuous RNA strand in the crystal structure described here, as opposed to a complementary DNA strand, is responsible for the difference remains to be determined.

Conclusion. In summary, we show that the hybrid octamer corresponding to the DNA−RNA junction formed during minus-strand synthesis by HIV-RT adopts a global A-type conformation in the crystal throughout its length. The cleavage site of HIV-RT RNase H is next to a base pair step with distinct stacking properties and variable backbone conformation, lending support to the hypothesis that these features are elements of the site recognition process.

ACKNOWLEDGMENT

We are grateful to A. Gonzalez for help with diffraction data collection at DESY, Hamburg, and to H. Sklenar and

Y. A. Muller (MDC, Berlin) for helpful comments on the manuscript.

REFERENCES

1. Skalka, A.-M., and Goff, S. P., Eds. (1993) *Reverse Transcriptase*, Cold Spring Harbor Laboratory Press, Cold Spring Harbor, NY.
2. Smith, J. S., and Roth, M. J. (1992) *J. Biol. Chem. 267*, 15071−15079.
3. Götte, M., Fackler, S., Hermann, T., Perola, E., Cellai, L., Gross, H. J., Le Grice, S. F. J., and Heumann, H. (1995) *EMBO J. 14*, 833−841.
4. Fedoroff, O. Y., Salazar, M., and Reid, B. R. (1996) *Biochemistry 35*, 11070−11080.
5. Berger, I., Kang, C. H., Sinha, N., Wolters, M., and Rich, A. (1996) *Acta Crystallogr. D52*, 465−468.
6. Otwinowski, Z. (1993) *DENZO: An Oscillation Data Processing Program for Macromolecular Crystallography*, Yale University Press, New Haven, CT.
7. Heinemann, U. (1991) *J. Biomol. Struct. Dyn. 8*, 801−811.
8. Navaza, J. (1994) *Acta Crystallogr. A50*, 157−163.
9. Jones, T. A., Zou, J.-Y., Cowan, S. W., and Kjeldgaard, M. (1991) *Acta Crystallogr. A47*, 110−119.
10. Brünger, A. T. (1992) *Nature 355*, 472−475.
11. Kleywegt, G. J., and Jones, T. A. (1996) *Acta Crystallogr. D52*, 826−828.
12. Brünger, A. T. (1992) *X-PLOR Manual*, version 3.1, Yale University Press, New Haven, CT.
13. Heinemann, U., Lauble, H., Frank, R., and Blöcker, H. (1987) *Nucleic Acids Res. 15*, 9531−9550.
14. Wang, A. H.-J., and Teng, M.-K. (1988) *J. Cryst. Growth 90*, 295−310.
15. Ramakrishnan, B., and Sundaralingam, M. (1993) *J. Biomol. Struct. Dyn. 11*, 11−26.
16. Wahl, M., and Sundaralingam, M. (1997) *Biopolymers 44*, 45−63.
17. Shakked, Z. (1991) *Curr. Opin. Struct. Biol. 1*, 446−451.
18. Wang, A. H.-J., Fujii, S., van Boom, J. H., van der Marel, G. A., van Boeckel, S. A. A., and Rich, A. (1982) *Nature 299*, 601−604.
19. Egli, M., Usman, N., Zhang, S., and Rich, A. (1992) *Proc. Natl. Acad. Sci. U.S.A. 89*, 534−538.
20. Gao, Y.-G., Robinson, H., van Boom, J. H., and Wang, A. H.-J. (1995) *Biophys. J. 69*, 559−568.
21. Portmann, S., Grimm, S., Workman, C., Usman, N., and Egli, M. (1996) *Chem. Biol. 3*, 173−184.
22. Horton, N. C., and Finzel, B. C. (1996) *J. Mol. Biol. 264*, 521−533.
23. Pley, H. W., Flaherty, K. M., and McKay, D. B. (1994) *Nature 372*, 68−74.
24. Teng, M.-k., Liaw, Y.-C., van der Marel, G. A., van Boom, J. H., and Wang, A. H.-J. (1989) *Biochemistry 28*, 4923−4928.
25. Woehrl, B. M., and Moelling, K. (1990) *Biochemistry 29*, 10141−10147.
26. Schatz, O., Mous, J., and Le Grice, S. F. J. (1990) *EMBO J. 9*, 1171−1176.
27. Jacobo-Molina, A., Ding, J., Nanni, R. G., Clark, A. D., Jr., Lu, X., Tantillo, C., Williams, R. L., Kamer, G., Ferris, A.L., Clark, P., Hizi, A., Hughes, S. H., and Arnold, E. (1993) *Proc. Natl. Acad. Sci. U.S.A. 90*, 6320−6324.
28. Saenger, W. (1984) *Principles of Nucleic Acid Structure*, Springer, New York.
29. Fedoroff, O. Y., Ge, Y., and Reid, B. R. (1997) *J. Mol. Biol. 269*, 225−239.
30. Salazar, M., Fedoroff, O. Y., Miller, J. M., Ribeiro, N. S., and Reid, B. R. (1993) *Biochemistry 32*, 4207−4215.
31. Fedoroff, O. Y., Salazar, M., and Reid, B. R. (1993) *J. Mol. Biol. 233*, 509−523.
32. Esnouf, R. M. (1997) *J. Mol. Graphics 15*, 132−134.
33. Merritt, E. A., and Murphy, M. (1994) *Acta Crystallogr. D50*, 869−873.
34. Lavery, R., and Sklenar, H. (1989) *J. Biomol. Struct. Dyn. 6*, 655−667.
35. Chandrasekaran, R., and Arnott, S. (1989) in *Landolt-Börnstein* (Saenger, W., Ed.) New Series, Group VII, Vol. 1b, pp 31−170, Springer, Berlin.

BI981152Y